Influence of the Rotor Slot Number on Core Losses of the Induction Motor

Bui Minh Dinh, Nguyen Viet Anh
School of Electrical Engineering and Electronics
Hanoi University of Science and Technology
Hanoi University of Industry
dinh.buiminh@hust.edu.vn

Abstract

Efficiency and back EMF are affected by the rotor slot number selection on the induction motor design. An analytical calculation will investigate the harmonic order of the air gap magnetic flux density back EMF with different geometrical parameters of rotor skewed angle considering the saturation of the induction motor. The Squirrel Cage Induction motor-SCIM with 36 stator slots/ 28,32 and 44 rotor bars are verified under starting and constant speed. Their electromagnetic characteristics, such as electromagnetic torque, stator current, and magnetic flux density are compared in between two configurations. The paper contributes that the proper rotor slot number selection has a strong impact on the induction motor and the best design is applied for a 10hp induction motor with fixed stator and rotor diameters.

Keywords
Electromagnetic force-EMF, Squirrel Cage Induction motor-SCIM

1. Introduction
The induction motor is being used in several applications. Such applications are various drives, such as pumps and ventilation. The design and analysis of electric machines were carried out with the use of equivalent circuits and analytical equations (McCoy 2009). The SCIM 7.5kW-4P was implemented by the same rotor diameter, the depth of the rotor bars, and the air-gap length. The stator used for the simulations is chosen from a real motor from industrial products, whose resistance was calculated through DC current injection and whose geometrical variables were known. The used motor is a 3-phase, 4-pole, 7.5 kW, and 380 V aluminum cast-cage induction motor (Prousalidis et al. 2010, Marques and Sousa 2010). The simulations carried out are AC time-harmonic and consider the nonlinear magnetic characteristic of the rotor and stator iron core (Charaabi 2012, Pyrhonen et al. 2008). This paper presents harmonic orders of the back EMF and the air gap magnetic flux density with analytical calculations. Then, the efficiency and torque and losses of some simulated induction motors with different rotor slot numbers have been shown and discussed. Three of the rotor slot selected numbers are 28, 32, and 40 with skewing rotor slots.

2. Machines Ratings and Specifications
This study is based on 36 stator slots and 32 rotor bars and the three-phase SCIM specification and ratings are shown in Figure 1 and Table 1.

© IEOM Society International

Figure 1. SCIM 7.5kW-4P

Air-gap eccentricity can be related to different manufacturing inaccuracies, such as construction tolerances, bearings, and shaft bending in J. Kappatou 2008. The eccentricity appears to some extends in all electrical machines and it has been studied from different points of view e.g. as related to its effect on the losses in J.-W. Kim 2005 or unbalanced magnetic pull.

Table 1. Technical parameters of SCIM 7.5 kW

Rated Output Power	7.5 kW
Number of Phases	3
Rated Voltage 400 V	380 VAC
Rated Current	15.7 A
Air gap	0.33mm
Stator Slot	36
Rotor bars	28,32 and 40

In Table.1 It is the assigned value of operation parameters used in motor design and Table. 2 is weight of variables and constraints are used for optimal design to improve the power factor and efficiency. These upper and lower limits are used fixed as GA then GA will optimize, and it should find optimal values at maximum efficiency and power factor. Then to perform the test convergence process if the optimal designed values are not achieved the motor initial design variables must be updated and fix the new population range within specified limits of individual variables then continue the optimization process and it should achieve optimal design values this optimal design values to shows better efficiency and power factor of SCIM until this process the algorithm cannot be terminated (Nandi 2004, Kim et al. 2005).

Table 2. Weight comparison of SCIM 7.5 kW

Components	**Materials**	**36Slot/28Bar**	**36Slot/32Bar**	**36Slot/40Bar**
Stator Lam (Back Iron)	M800-50A	**12.92**	12.92	12.92
Stator Lam (Tooth)	M800-50A	5.523	5.523	5.523
Armature Winding [Active]	Copper (Pure)	2.67	2.67	2.67

Armature EWdg [Front]	Copper (Pure)	1.475	1.475	1.475
Armature EWdg [Rear]	Copper (Pure)	1.475	1.475	1.475
Rotor Lam (Back Iron)	M800-50A	3.804	3.804	4.326
Rot Inter Lam (Back Iron)		1.73E-05	1.73E-05	1.97E-05
Rotor Lam (Tooth)	M800-50A	5.496	5.429	5.148
Rotor Cage Top Bar	Aluminium	1.105	1.132	1.036
Rotor Cage Top Bar Opening	Aluminium	0.01059	0.01059	0.01059
Rotor Cage (Front End)	Aluminium	0.3109	0.3109	0.2962
Rotor Cage (Rear End)	Aluminium	0.3109	0.3109	0.2962
Rotor Cage		1.738	1.764	1.639
Total		37.27	37.23	37.35

3. FEM Model

A 2-dimensional (2D) view of the SCIM FEM model developed is given in Fig. 3
A 2-dimensional (2D) view of the SCIM FEM model developed is given in Fig. 3
A 2-dimensional (2D) view of the SCIM FEM model developed is given in Fig. 3
A 2-dimensional (2D) result of the SCIM FEM model developed is given in Figure 3. The rotor position is rotated from 0◦ to 360◦. The electromagnetic forces (back EMF) generated at each rotor position is determined and is plotted in Figure 2.

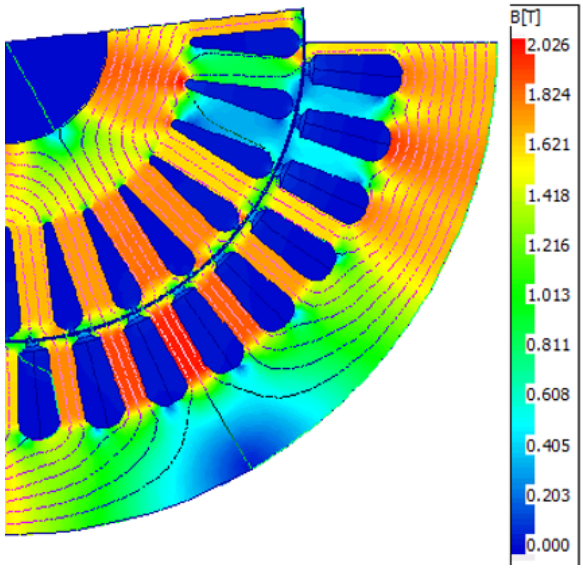

Figure 2. Flux density of 7.5kW-4P

This simulation is performed to find out what the rotor skewing angle is when back EMF is almost sinusoidal. For the straight-slot-type rotor of the IM machine, if we divide the mechanical rotating degree θ into N equal parts, and simultaneously calculate the straight-slot-type back-EMF waveform with different mechanical rotating degree 0, θ/N, 2θ/N, . . . , θ, the relationship between skewed-slot-type back-EMF waveform and straight-slot-type back-EMF waveform can be written as follows:

$$e_{sk}(\theta) = \frac{1}{N+1}\left(\sum_{k=0}^{N} e_{st}(\theta_k)\right) \quad (1)$$

where $e_{sk}(\theta)$ is the skewed-slot-type back EMF, $e_{st}(\theta_k)$ is the straight-slot-type back EMF and $\theta_k = k\theta/N$

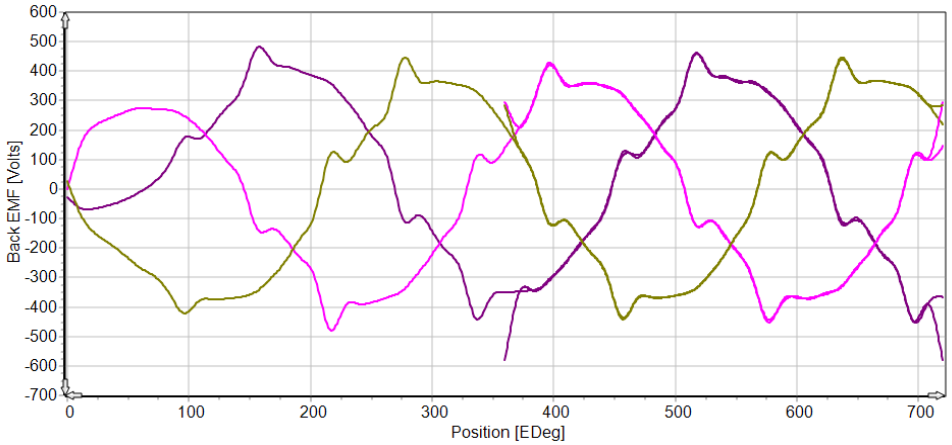

a) Back EMF unskewed

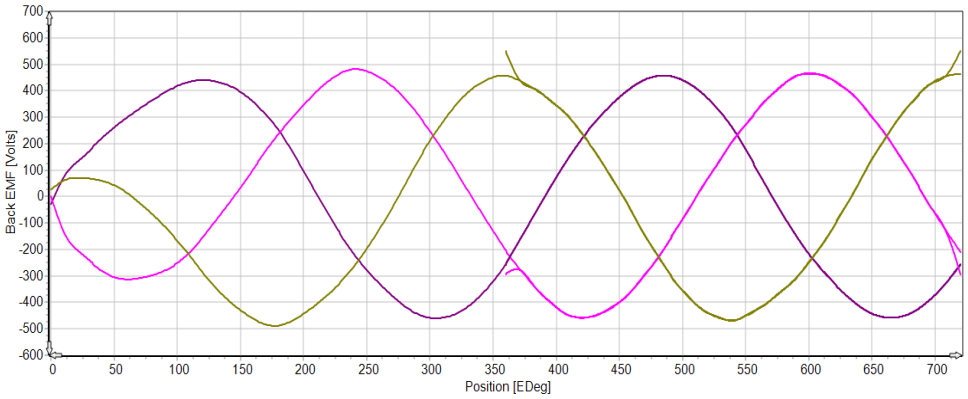

b) Back EMF skewed ¾ rotor slot

Figure 3. Back EMF of 7.5kW-4P

Figure 3 shows the analysis of back EMF waveforms of the straight-slot-type rotor and skewed-slot-type rotor (3/4 slot). From Figure 3b, it can be seen that the harmonics are very significant in the back EMF waveforms of the straight-slot-type rotor, and the harmonics are the main components in the back EMF waveforms of the skewed-slot-type rotor. In general, the total harmonic distortion (THD) of the back EMF waveforms of the IM machine with the skewed-slot-type rotor is 1.79%. To verify the simulations, three models have compared some outputs such as torque, power, and efficiency with different rotor bar numbers.

Table 3. Electromagnetic result comparison

Parameter	36Slot/28Bar	36Slot/32Bar	36Slot/40Bar	Unit
Airgap Torque (on load)	50.676	50.486	50.705	Nm
Shaft Torque	49.777	49.692	49.915	Nm

Requested on load power	7500	7500	7500	Watts
Output Mechanical Power	7500.8	7501	7500.7	Watts
Input Active Electrical Power (from Power Balance)	8527.5	8500.8	8526.9	Watts
Input Active Electrical Power (ideal)	8778.9	8758.6	8773.6	Watts
Total Losses (Analytic on load)	1026.7	999.83	1026.2	Watts
Input Reactive Power (on load)	4978.5	5077	4885.3	VA
Apparent Power	10092	10124	10042	VA
Power Factor (on load) (Phasor)	0.86986	0.86516	0.87369	
System Efficiency	88.96	89.239	87.966	

4. Method for iron loss calculation

The iron loss per unit weight in the case of a single-frequency alternating magnetic field can be expressed approximately as follows:

$$w_i = K_e f^2 B_{max}^2 + K_h f B_{max}^2 \tag{2}$$

where f is the frequency, and K_e and K_h are the constant obtained by the Epstein frame test
However, the real magnetic field in the rotating machine can be considered to be complex. It includes many harmonics, especially near the air gap. Furthermore, the direction of the magnetic field vector is not constant.

5. Measured and Calculated Results

the experimental and calculated iron losses at synchronous speed. The results calculated while neglecting the harmonics are also plotted for comparison. The experimental iron loss defined by the classical electric machine theory is where W_{noload} is the no load loss;

$$W_i = W_{noload} - W_1 - W_m \tag{3}$$

In the calculation of the total loss, the mechanical loss is estimated as

$$W_m = 8d(l + 0.15)v^2 \tag{4}$$

where d is the diameter of the rotor, l is the core length, and v is the velocity on the surface of the rotor. This expression has been obtained from various experiments and is widely used in the design of rotating machines.

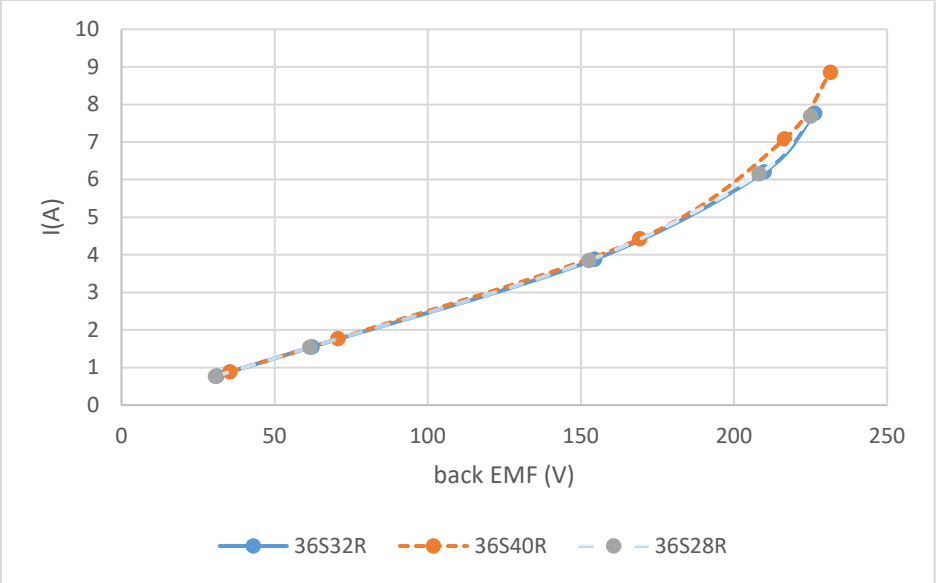

Figure 4. No load current vs back EMF

Table 4 Magnetizing current results

Line Current (rms) (on load)	15.279	16.349	15.977
Phase Current (rms) (on load)	15.279	16.349	15.977
Referred Rotor Current (rms) (on load)	13.576	13.987	13.572
Rotor Bar Current (rms) (on load)	335.07	345.21	334.97
Endring Current (rms) (on load)	752.89	775.69	752.66
Magnetizing Current (no load)	6.3499	6.0963	6.0963
Magnetizing Current (rms) (on load)	5.3684	6.7167	6.7731
Core Loss Current (rms) (on load) (T circuit)	0.068403	0.07103	0.071088
Core Loss Current (rms) (on load) (L circuit)	0.066004	0.068104	0.06819

© IEOM Society International

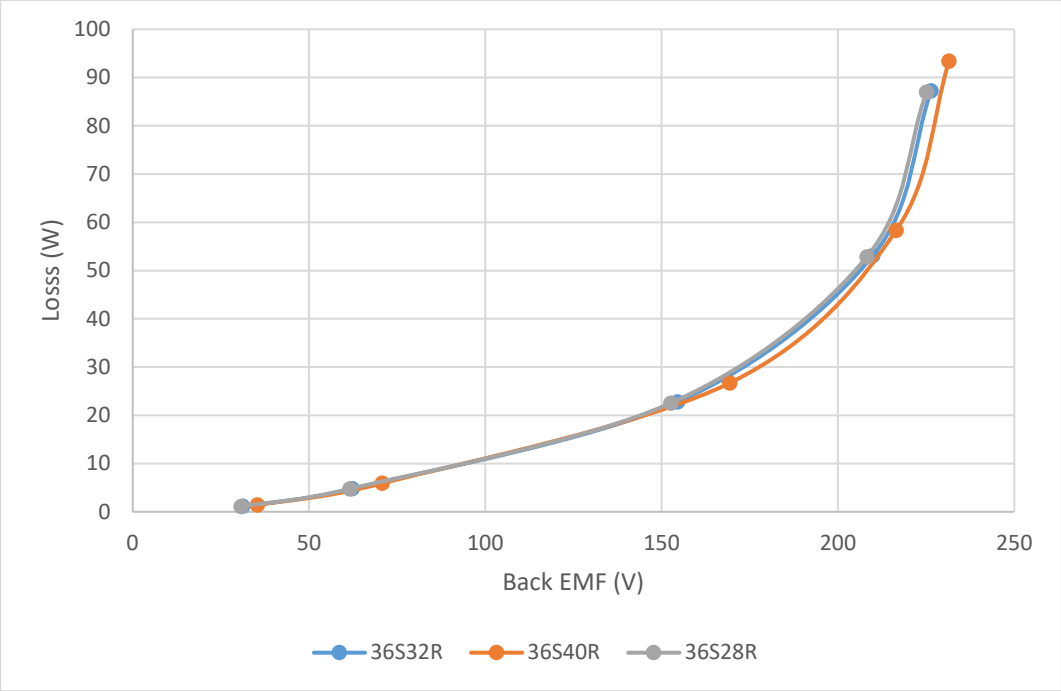

Figure 5. Core loss power vs back EFM

The iron loss results of three motors in the figure. 5 show good agreement, verifying the validity of the proposed calculation method. Among the calculated results, the case of the cage rotor with skew shows the largest calculation error, with a calculated value 14% less than the experimental result. It can be considered that this error is caused by neglect of the inter-bar currents in the calculation (Kappatou 2008, Boldea 2010, Gierras 2006).

6. Conclusions

This paper has analyzed and compared the electromagnetic performance of three induction motors for industrial applications. The 32-rotor bar has the lowest iron loss. To verify the proposed design, a detailed design of a 3-phase 36-slot and 4-pole IM is assembled and verified torque, power, and efficiency performances. The back EMF waveforms have been analyzed based on the FEA modeling. The thermal simulation was implemented to validate overheat capacity

Acknowledgments

This research was supported Institute for Control Engineering and Automation- ICEA)-HUST, Hanoi Electromechanical Manufacture-HEM, WOLONG Motor and Viettel High Tech -VHT for High Processing Speed Computer to run software and analytical program in MATLAB coupling to CAD, FEMM in this study.

References

McCoy, T. J. and Amy J. V. Jr., The state-of-the-art of integrated electric power and propulsion systems and technologies on ships, *in Proceedings of the IEEE Electric Ship Technologies, Symposium (ESTS '09),* pp. 340–344, April 2009.

Prousalidis J. M. and Mouzakis, P. S., Analysis of electric power demands of podded propulsors*, Journal of Marine Engineering and Technology,* vol. 2010, no. 16, pp. 3–13, 2010.

Marques G. D. and Sousa, D. M., A new sensor less MRAS based on active power calculations for rotor position estimation of a DFIG, *Advances in Power Electronics*, vol. 2011, Article ID 970364, 8 pages, 2011.

Charaabi, L., FPGA-based fixed point implementation of a realtime induction motor emulator*, Advances in Power Electronics,* vol. 2012, Article ID 409671, 10 pages, 2012.

Pyrhonen, J., Jokinen, T. and Hrabovcova, V., Design of Rotating Electrical Machines, *John Wiley & Sons*, 1st edition, 2008.

Nandi, S., Modeling of induction machines including stator and rotor slot effects, *IEEE Transactions on Industry Applications*, vol. 40, no. 4, pp. 1058–1065, 2004.

Kim, J.-W., Kim, B.-T. and Kwon, B. I., Optimal stator slot design of inverter-fed induction motor in consideration of harmonic losses, *IEEE Transactions on Magnetics,* vol. 41, no. 5, pp. 2012–2015, 2005.

Kappatou, J., Gyftakis, K. and Safacas, A., FEM study of the rotor slot design influences on the induction machine characteristics, in Studies in Applied Electromagnetics and Mechanics, *Advanced Computer Techniques in Applied Electromagnetics,* IOS Press, vol. 30, 2008.

Boldea, I. and Nasar, S. A., The Induction Machines Design Handbook, *Taylor & Francis Group*, 2010.

Gierras, J. F., Wang, C. and Lai, J. C., Noise of Polyphase Electric Motors, *CRC Press,* 2006.

© IEOM Society International